

Design of potent and selective hybrid inhibitors of the mitotic kinase Nek2: SAR, structural biology and cellular activity[†]

Paolo Innocenti,[‡] Kwai-Ming J. Cheung,[‡] Savade Solanki,[‡] Corine Mas-Droux,[§] Fiona Rowan,^{‡,§} Sharon Yeoh,[¶] Kathy Boxall,[‡] Maura Westlake,[‡] Lisa Pickard,[‡] Tara Hardy,[¶] Joanne E. Baxter,[¶] G. Wynne Aherne,[‡] Richard Bayliss,^{§,¶} Andrew M. Fry,[¶] and Swen Hoelder^{,‡}*

The Institute of Cancer Research, Division of Cancer Therapeutics, Cancer Research UK Cancer Therapeutics Unit, 15 Cotswold Road, Sutton, Surrey SM2 5NG, United Kingdom, The Institute of Cancer Research, Division of Structural Biology, Chester Beatty Laboratories, 237 Fulham Road, London SW3 6JB, United Kingdom, Department of Biochemistry, University of Leicester, Henry Wellcome Building, Lancaster Road, Leicester, LE1 9HN, United Kingdom.

RECEIVED DATE (to be automatically inserted after your manuscript is accepted if required according to the journal that you are submitting your paper to)

[†]Atomic coordinates and structure factors for the crystal structure of ligand bound Nek2 can be accessed using the following PDB codes: **rac-17j** (4A4X), **rac-21** (4AFE).

*To whom correspondence should be addressed. Phone, +44 20 87224353; e-mail, swen.hoelder@icr.ac.uk.

[‡]The Institute of Cancer Research, Division of Cancer Therapeutics.

[§]The Institute of Cancer Research, Division of Structural Biology.

[†]Department of Biochemistry, University of Leicester.

Abbreviations: Abl, Abelson murine leukemia viral oncogene; ATP, adenosine triphosphate; AurA, Aurora A; CDK2, cyclin-dependent kinase 2; C-Nap1, centrosomal Nek2-associated protein 1; DCE, 1,2-dichloroethane; DCM, dichloromethane; DME, 1,2-dimethoxyethane; DMF, *N,N*-dimethylformamide; DFG, Asp-Phe-Gly; Hec1, highly expressed in cancer 1; DMSO, dimethyl sulfoxide; HMGA2, high mobility group AT-hook 2; Lck, lymphocyte-specific protein tyrosine kinase; LE, ligand efficiency; Mad, mitotic arrest deficient-like; MPS-1, human monopolar spindle 1; Nek, NIMA (never in mitosis gene a)-related kinase; Nlp, ninein-like protein; PAMPA, parallel artificial membrane assay; Plk, polo-like kinase; PMB, *para*-methoxybenzyl; SAC, spindle assembly checkpoint; SAR, structure-activity relationship; SD, standard deviation; TFA, trifluoroacetic acid; THF, tetrahydrofuran.

Abstract

We report herein a series of Nek2 inhibitors based on an aminopyridine scaffold. These compounds have been designed by combining key elements of two previously discovered chemical series. Structure based design led to aminopyridine (**R**)-**21**, a potent and selective inhibitor able to modulate Nek2 activity in cells.

Introduction

(Never in mitosis gene a)-related kinase-2 (Nek2) is a serine/threonine kinase involved in key mitotic processes. It localizes to the centrosomes, and takes part in the regulation of spindle pole organization and separation by phosphorylation of centrosomal Nek2-associated protein 1 (C-Nap1), rootletin, and ninein-like protein (Nlp).¹ Nek2 has also been reported to act as a regulator of the spindle assembly checkpoint (SAC) through interaction or phosphorylation of highly expressed in cancer 1 (Hec1), mitotic arrest deficient-like 1 (Mad1), and mitotic arrest deficient-like 2 (Mad2).² In recent publications,

the role of Nek2 was probed by RNAi knockdown experiments and through inhibition by a covalent inhibitor. These studies suggest that Nek2 is not essential for centrosome separation but plays a supportive part.³ Moreover, definitive evidence for a role in the SAC is still lacking. Despite recent and somewhat conflicting literature reports on its requirement for mitotic progression, Nek2 is an interesting cancer target. High levels of Nek2 expression have been found in many tumors, and RNAi knockdown experiments have shown antiproliferative effects in HeLa, MDA-MB-231, HuCCT1 and MCF7 cells *in vitro* as well as *in vivo*.⁴

The paucity of potent, selective and cell-active inhibitors has hampered in-depth investigation of the role of Nek2. Recently, propynamide **1** has been shown to be a nanomolar range inhibitor acting through an irreversible mechanism (Figure 1).^{3a} We previously described a pyrazine series of Nek2 inhibitors (exemplified by **2**, Figure 1) that attained an IC₅₀ value of 0.23 μ M, displayed high selectivity, but failed to achieve cellular activity due to poor permeability.⁵ In addition, we published results of a series of benzimidazole compounds that showed comparable activity towards Nek2 and good permeability (see structure (**R**)-**3**, Figure 1).⁶

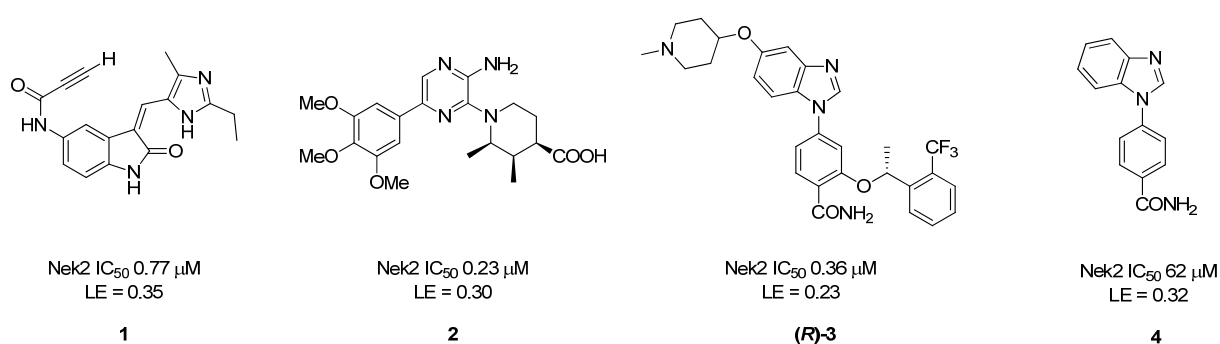


Figure 1. Nek2 inhibitors described in the literature.

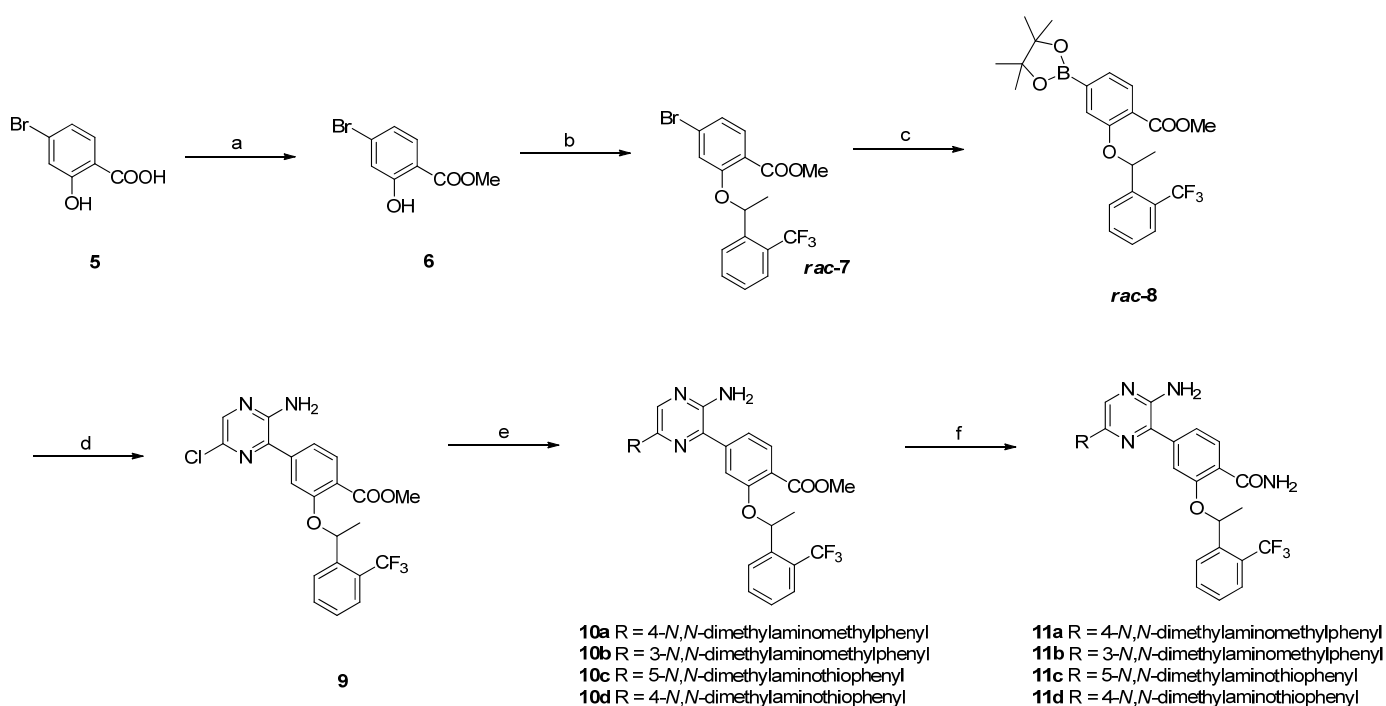
The structure-activity relationship (SAR) of this series was found to be non-linear: high Nek2 inhibition was achieved when the basic piperidine and the fully substituted benzyl ether were present in the same molecule. Removal of either group resulted in a significant drop in potency. Despite these interesting features, these compounds also did not show any cellular activity, most likely due to lack of

sufficient potency. Herein we report the exploration of hybrids of the two series that ultimately led to potent compounds with the ability to modulate the phosphorylation status of a Nek2 substrate in cells.

Chemistry

The pyrazine compounds were prepared starting from commercially available methyl 4-bromo-2-hydroxybenzoic acid **5**, which was transformed into methyl ester **6** by treatment with sulfuric acid in methanol (Scheme 1). Introduction of the benzyl ether functionality to afford compound *rac*-**7** was carried out under Mitsunobu conditions⁷ in the presence of (±)-1-(2-(trifluoromethyl)phenyl)ethanol, whereas transformation into the corresponding boronic acid ester *rac*-**8** was accomplished by means of a standard palladium catalyzed reaction.⁸ Coupling with known 3-bromo-5-chloropyrazin-2-amine⁹ afforded chloroderivative **9**, which was further elaborated through Suzuki reactions to produce esters **10** (Scheme 1).¹⁰ The boronic acids or esters required for the couplings described above were either commercially available or prepared according to standard procedures.¹¹ Finally, esters **10** were heated with ammonia in methanol to give primary amides **11** (Scheme 1).

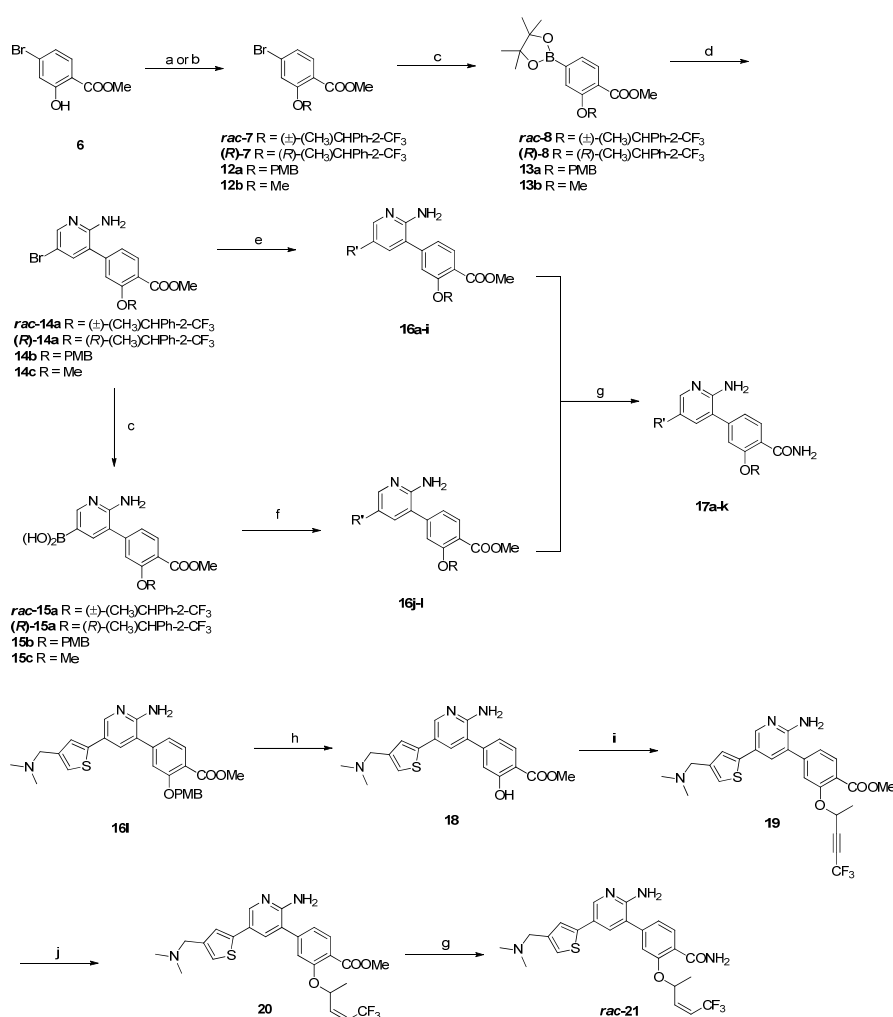
Scheme 1. Synthesis of aminopyrazines^a



^a Reagents and conditions: a) H₂SO₄, MeOH, 80 °C; b) (±)-1-(2-(trifluoromethyl)phenyl)ethanol, di-*tert*-butyl azodicarboxylate, PPh₃, DCM, 0 °C to rt; c) bis(pinacolato)diboron, NaOAc, Pd(dppf)Cl₂·DCM, DMF, μ W, 100 °C; d) 3-bromo-5-chloropyrazin-2-amine, NaHCO₃, Pd(dppf)Cl₂·DCM, DMF/water, μ W, 100 °C; e) RB(OR)₂ or RB(OH)₂, Na₂CO₃, Pd(PPh₃)₄, DMF/water, μ W, 125-135 °C; f) NH₃, MeOH, 75-90 °C.

The aminopyridine series was made by a synthetic sequence similar to that used for the aminopyrazine series. Ethers **7** and **12a** were prepared starting from phenol **6** under Mitsunobu conditions with (±)-, (*S*)-1-(2-(trifluoromethyl)phenyl)ethanol or 4-methoxybenzyl alcohol (Scheme 2). Ether **12b** was made from compound **6** by treatment with methyl iodide and potassium carbonate. Boronic esters **8** and **13** were formed using standard palladium chemistry⁸ and subsequently coupled with 5-bromo-3-iodopyridin-2-amine under Suzuki conditions to afford bromopyridines **14**.¹⁰

Scheme 2. Synthesis of aminopyridines^a



ester	amide	R	R'
16a	17a	(±)-(CH ₃)CHPh-2-CF ₃	
16b	17b	(±)-(CH ₃)CHPh-2-CF ₃	
16c	17c	(±)-(CH ₃)CHPh-2-CF ₃	
16d	17d	(±)-(CH ₃)CHPh-2-CF ₃	
16e	17e	(±)-(CH ₃)CHPh-2-CF ₃	
16f	17f	(±)-(CH ₃)CHPh-2-CF ₃	
16g	17g	(±)-(CH ₃)CHPh-2-CF ₃	
16h	17h	(±)-(CH ₃)CHPh-2-CF ₃	
16i	17i	Me	
rac-16j	rac-17j	(±)-(CH ₃)CHPh-2-CF ₃	
(R)-16j	(R)-17j	(R)-(CH ₃)CHPh-2-CF ₃	
16k	17k	Me	
16l	-	PMB	

^a Reagents and conditions: a) (±)-, (*S*)-1-(2-(trifluoromethyl)phenyl)ethanol or 4-methoxybenzyl alcohol, di-*tert*-butyl azodicarboxylate, PPh₃, DCM, 0 °C to rt (*rac*-**7**, (*R*)-**7** and **12a**); b) MeI, K₂CO₃,

DMF, rt (**12b**); c) bis(pinacolato)diboron, NaOAc, Pd(dppf)Cl₂·DCM, DMF, μ W, 100 °C; d) 5-bromo-3-iodopyridin-2-amine, NaHCO₃, Pd(dppf)Cl₂·DCM, DMF/water, μ W, 100 °C; e) RB(OR)₂ or RB(OH)₂, Na₂CO₃, Pd(PPh₃)₄, DMF/water or DME/water, μ W, 110-135 °C (**16a-i**); f) 1-(5-bromothiophen-3-yl)-*N,N*-dimethylmethanamine, Na₂CO₃, Pd(PPh₃)₄, DME/water, μ W, 110 °C (**16j-l**); g) NH₃, MeOH, 70-80 °C; h) TFA, DCM, 0 °C; i) (\pm)-5,5,5-trifluoropent-3-yn-2-ol, di-*tert*-butyl azodicarboxylate, PPh₃, DCM, 0 °C to rt; j) H₂, Lindlar's catalyst, MeOH, rt.

Aminopyridines **16a-i** were formed by Suzuki coupling of the appropriate boronic esters or acids with bromoderivatives **14** (Scheme 2).^{10,12} Derivatives **16j-l** were prepared starting from 1-(5-bromothiophen-3-yl)-*N,N*-dimethylmethanamine¹³ and suitably prepared boronic acids **15**.¹⁰ Ammonolysis of esters **16** furnished the target primary amides **17**. Compound **21** was prepared *via* a slightly different route: aminopyridine **16l** was deprotected with trifluoroacetic acid to afford phenol **18**, which was derivatized with (\pm)-5,5,5-trifluoropent-3-yn-2-ol¹⁴ under Mitsunobu conditions to give ether **19**. Target amide *rac*-**21** was obtained after hydrogenation with Lindlar catalyst to afford ester **20** followed by ammonolysis (Scheme 2).

Results and discussion

Hybrid compounds design

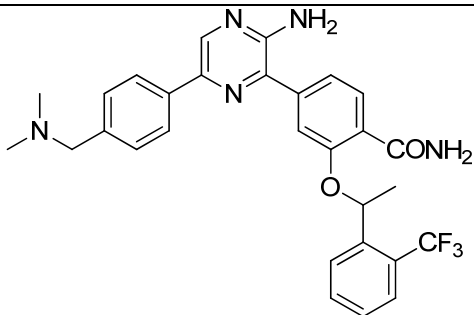
As mentioned above, our previous studies of the benzimidazole series led to permeable and selective inhibitors which suffered from insufficient potency and high lipophilicity (compound (*R*)-**3**, Figure 1).⁶ Our results indicated that the poor ligand efficiency (LE) and modest potency of these compounds were at least in part due to inefficient binding of the phenyl substituted benzimidazole core **4** (IC₅₀ value of 62 μ M, LE = 0.32, Figure 1). We speculated that a more potent compound could be obtained if the substituents of benzimidazole **3** were to be grafted on a core that binds more efficiently to the hinge region of Nek2. A replacement candidate for the benzimidazole moiety was the aminopyrazine-type scaffold, which in our studies consistently showed better LE compared to the benzimidazoles. Indeed, superposition of co-crystal structures of both series indicated that hypothetical hybrids of these series can address all the pharmacophoric features of benzimidazole (*R*)-**3** (Figure 2A). This prompted us to prepare a series of compounds exploring this design principle and comprising the following key

features: the presence of a suitably placed amino-substituted aromatic group, an aminopyrazine-type binding scaffold and a phenyl carboxamide substituted with a benzyl ether (Figure 1).

SAR of benzyl ether-substituted hybrid compounds

The initial series of compounds were built by fusing the hinge-binding fragment of aminopyrazine **2** with the benzyloxy-substituted benzamide moiety of benzimidazole (**R**)-**3** (Figure 1). In order to place a suitable basic residue mimicking the piperidine ring of compound (**R**)-**3**, a *para*-*N,N*-dimethylaminomethylphenyl group was used instead of the trimethoxyphenyl substituent. The resulting hybrid **11a** showed a Nek2 IC₅₀ value of 0.79 μM (Table 1) and proved to be approximately equipotent to the parent compounds (0.23 μM and 0.36 μM, respectively, for pyrazine **2** and benzimidazole (**R**)-**3**, Figure 1). Moving the amino group attachment point to the *meta* position resulted in aminopyrazine **11b** which demonstrated reduced Nek2 inhibition (IC₅₀ value of 2.47 μM, Table 1). During the course of previous studies on the aminopyrazine series, it was found that switching to an aminopyridine hinge-binding scaffold caused a marked increase in Nek2 inhibition.^{15,12} For this reason, aminopyridines **17a** and **17b** were prepared, featuring a *para*- and a *meta*-substituted phenyl ring moiety, respectively. Gratifyingly, both compounds showed improved activity against Nek2 with IC₅₀ values of 0.12 and 0.21 μM, respectively (Table 1). Overall, these hybrid compounds showed moderate activity and LE as well as high predicted lipophilicity (Table 1).

Table 1. Phenyl substituted hybrids^a

compound		Nek2 IC ₅₀ (μM)	LE	Plk1 IC ₅₀ (μM)	CLogP
11a		0.79 ± 0.31	0.21	3.90	5.18

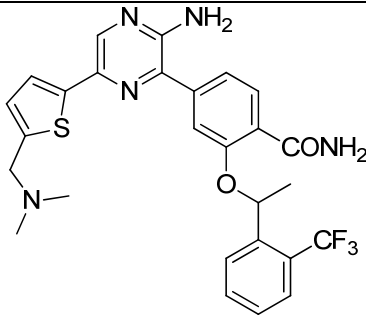
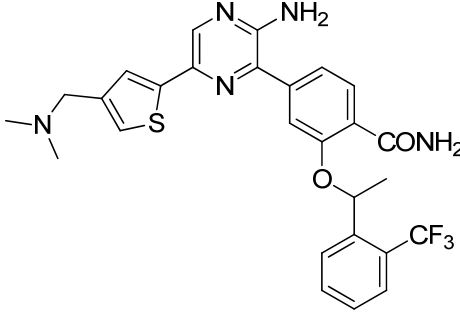
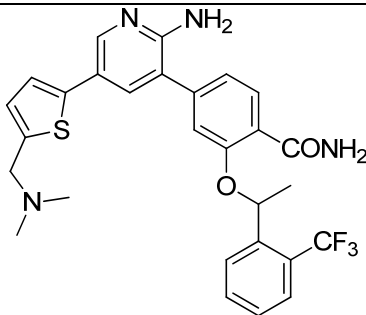
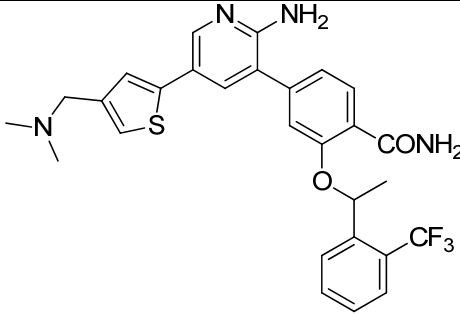
11b		2.47 ± 0.66	0.20	12.1	5.18
17a		0.12 ± 0.01	0.24	1.56 ± 0.18	5.47
17b		0.21 ± 0.03	0.24	3.29 ± 1.22	5.47

^a Results are mean (\pm SD) for $n \geq 3$, or mean values of two independent determinations with individual determinations in parentheses or samples run $n = 1$; compounds are racemic unless otherwise stated.

In order to improve the potency of this series against Nek2, the aminomethyl-substituted phenyl ring was replaced by an isosteric thiophene. Whereas in a previous series this modification had a generally positive effect on Nek2 activity,⁵ these results showed that the outcome strongly depends on hinge-binding motif (Table 2). Thus, introduction of an α' - or β' -aminomethyl substituted α -thiophene on the aminopyrazine scaffold resulted in a drop in Nek2 inhibition, with compounds **11c** and **11d** showing IC₅₀ values of 2.68 and 2.63 μ M, respectively (Table 2; compare with aminopyrazines **11a** and **11b**, Table 1). Conversely, when the same change was applied on the aminopyridine core, a significant improvement in activity towards Nek2 was observed: the IC₅₀ values for compounds **17c** and *rac*-**17j**, featuring an α' - or β' -aminomethyl substituent, are 0.047 and 0.059 μ M respectively (Table 2). Further

decoration of the thiophene group of aminopyridine **17c** with methyl substituents either at the β' or β position resulted in virtually equipotent compounds: the IC_{50} values for aminopyridines **17d** and **17e** are 0.047 and 0.058 μM , respectively (Table 3).

Table 2. Thiophene substituted hybrids^a

compound		Nek2 (μM)	IC_{50}	LE	Plk1 (μM)	IC_{50}	CLogP
11c		2.68 ± 1.68		0.20	-		5.21
11d		2.63 ± 1.42		0.20	-		5.13
17c		0.047 ± 0.015		0.27	0.50 ± 0.12		5.50
rac-17j		0.059 ± 0.016		0.26	1.32 ± 0.34		5.42

^a Results are mean (\pm SD) for $n \geq 3$, or mean values of two independent determinations with individual determinations in parentheses or samples run $n = 1$; compounds are racemic unless otherwise stated.

Table 3. SAR around the thiophene core^a

compound		Nek2 IC50 (μ M)	LE	CLogP
17d		0.047 ± 0.005	0.26	5.99
17e		0.058 ± 0.020	0.25	5.99
17f		0.093 ± 0.017	0.24	6.42
17g		0.318 ± 0.060	0.22	5.19

^a Results are mean (\pm SD) for $n \geq 3$, or mean values of two independent determinations with individual determinations in parentheses or samples run $n = 1$; compounds are racemic unless otherwise stated.

Next, we prepared two additional compounds bearing alterations of the basic residue: compound **17f** features a cyclic, more rigid amino group, while compound **17g** features a less basic morpholine ring. The former did show only a slight decrease in Nek2 inhibition (IC_{50} for **17f** is 0.093 μ M, Table 3) suggesting that the shape of the aminomethyl substituent is not crucial for activity. Conversely, the reduced basicity of aminopyridine **17g** had a more pronounced effect, with the IC_{50} value increasing more than 7-fold to 0.318 μ M (compare compound **17c** and **17g**, Tables 2 and 3). These observations are in line with previous findings on the role of amino substituents in benzimidazole-based Nek2 inhibitors, and stress the importance of a suitably placed basic residue with the ability to engage in charge-charge type interactions.⁶

Since this series was initially inspired by Plk1 inhibitors¹⁶ and still maintained the original substituted benzyl ether moiety, we investigated the Plk1 inhibition for selected compounds. Whilst all showed a preference for Nek2, the window was relatively small: Plk1 IC_{50} values were 3.90, 1.56 and 1.32 μ M, respectively, for amides **11a**, **17a** and *rac*-**17j**, which translated to 10- to 25-fold reduced activity when compared to Nek2 (Tables 1 and 2). Since we were interested in developing tool compounds and Plk1 has been suggested to play a role upstream of Nek2,^{3b} an improved selectivity window was desirable. In addition, we were still concerned about the high lipophilicity of the described compounds.

Co-crystal structure of aminopyridine *rac*-**17j** bound to Nek2

In order to address these issues, we solved the co-crystal structure of *rac*-**17j** bound to Nek2. As expected from our design hypothesis leading to this hybrid series, the binding mode shares many features with that of *rac*-**3**, including a DFG-out conformation of the kinase.⁶ Here, we will focus on key elements. The aminopyridine forms two hydrogen bonds with the hinge region at Glu87 and Cys89 (Figure 2B and 2C), compared to the single hydrogen bond formed between the imidazole ring of *rac*-**3** and Cys89. The phenyl ring of the substituted benzamide sandwiches between the gatekeeper Met86, and Phe148, whilst the amide group engages in two hydrogen bonds with the backbone NH and the side

chain carbonyl group of Asp159 of the DFG motif. As observed for *rac-3*, the substituted benzyl group is well ordered with the trifluoromethyl group binding to a hydrophobic pocket formed by part of the glycine rich loop, and one of the fluorine atoms is engaged in an orthogonal interaction with the carbonyl group of Ile14 (3.6 Å). The position of the methyl group clearly reveals the *R* configuration at the benzylic stereocentre of *rac-17j* even though the racemic mixture was used for the soaking process.

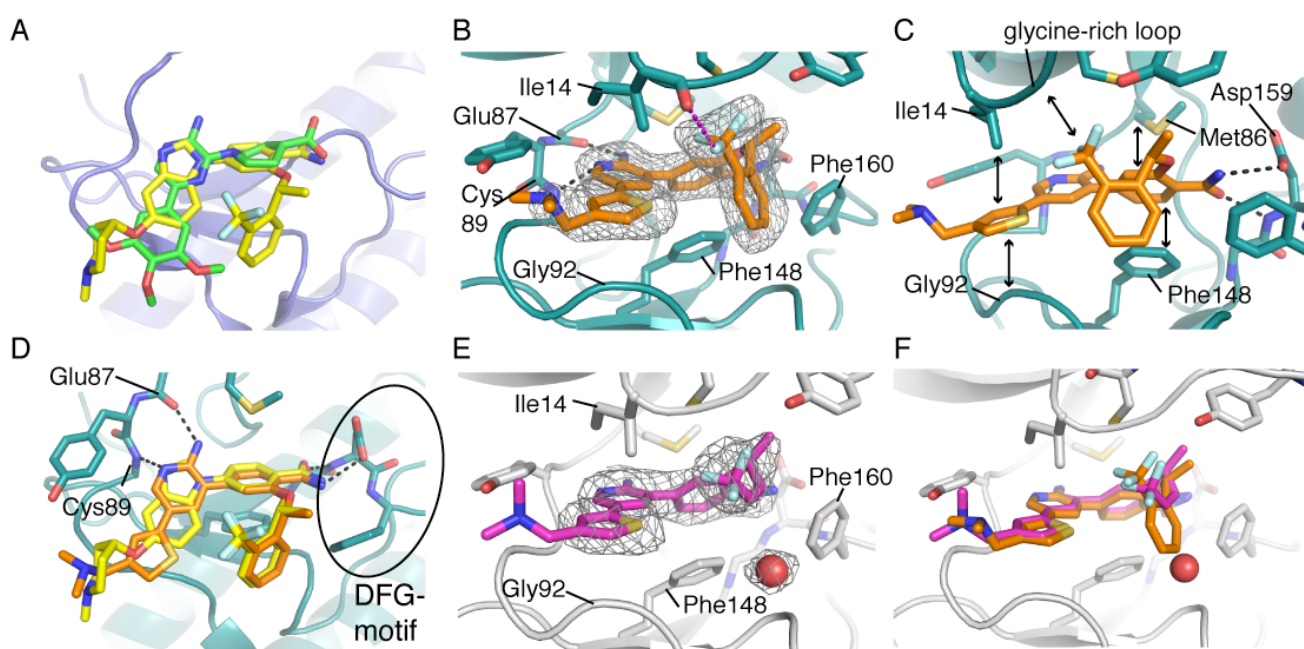


Figure 2. The structures of aminopyridines *rac-17j* and *rac-21* bound to Nek2 as determined by X-ray crystallography. (A) The rational basis of the hybrid design is illustrated by the superposition of the structure of Nek2 (purple) bound to *rac-3* (carbons colored yellow), extracted from PDB code 2XNP, on the structure of Nek2 (not shown) bound to an aminopyrazine inhibitor (carbons colored green), PDB code 2XKF. (B) View of the ATP binding site of Nek2 (carbons colored teal) occupied by aminopyridine *rac-17j* (carbons colored orange). Wire-mesh represents the 2mFo-DFc electron density map in the vicinity of the compound, contoured at 1.0 σ . Black dashed lines represent hydrogen bonds formed between the protein and the compounds, magenta dashed lines represent the orthogonal interaction between Ile14 and the trifluoromethyl group. (C) The structure viewed in a second orientation, showing the hydrophobic contacts between the compound and protein (double-headed arrows) and the hydrogen bonds between the amide group of the compound and Asp159 of the Nek2

DFG motif (black dashed lines). (D) Superposition of structures of compound **rac-17j** bound to Nek2 (teal) and compound **rac-3** (PDB code 2XNP, carbons colored yellow) bound to Nek2 (not shown), viewed from above. (E) The structure of **rac-21** (carbons colored magenta) bound to Nek2 (light gray). An ordered water molecule in the active site is shown as a red sphere. Wire-mesh represents the 2mFo-DFc electron density map in the vicinity of the compound and the water molecule, contoured at 1.0 σ . (F) Superposition of the structures of Nek2 (light gray) bound to **rac-21** with the structure of Nek2 (not shown) bound to **rac-17j**.

This confirmed that the *R* isomer is the most potent enantiomer for Nek2 binding as observed for the benzimidazole series.⁶ The thiophene ring engages in hydrophobic contacts with Ile14 and Gly92. The dimethylamino group is clearly resolved and superimposes well with the basic center of the piperidine ring of **rac-3** (Figure 2D). We have shown that the correct positioning of the piperidine ring of **rac-3** is crucial for high selectivity of this compound against Plk1 most likely by causing a clash with the Arg136 residue in Plk1.⁶ We hypothesize that the *N,N*-dimethylamino group of **rac-17j** plays a similar role, leading to the 25-fold selectivity with respect to Plk1 inhibition. The observation that **rac-17j** shows a somewhat smaller selectivity window might be explained by the smaller size of the dimethylamino group compared to the piperidine group leading to reduced steric interaction with Arg136 in Plk1.

The binding mode revealed by the crystal structure thus confirmed our design hypothesis. However, we were keen to further improve the selectivity against Plk1 and to reduce the lipophilicity of our compounds. Our attention turned to the role of the benzyl ether moiety. Close examination of the X-ray co-crystal structures of **rac-17j** and **rac-3** revealed that this aromatic region is solvent exposed and has few contacts with Nek2 (Figure 2B and 2D). Its main role appears to be as a scaffold for the trifluoromethyl group that binds to the small hydrophobic groove formed partially by the Gly rich region. As we have previously shown, the benzylic methyl group is important for activity since it stabilizes the bioactive conformation in which the fluorinated moiety points towards the groove through

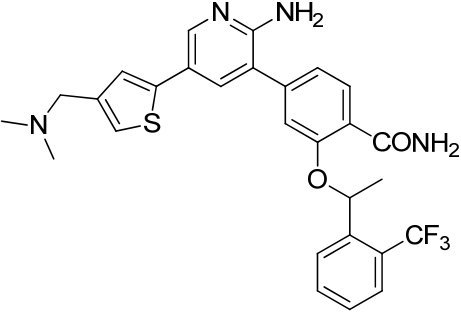
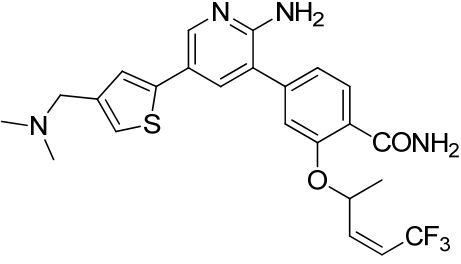
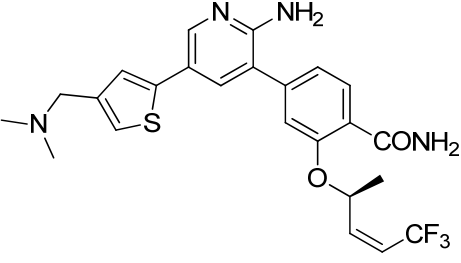
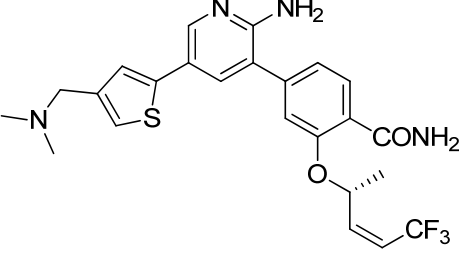
minimization of the 1,3-allylic strain.⁶ We hypothesized that the phenyl group is not needed for potent Nek2 inhibition and can be replaced by a smaller moiety that leads to comparable positioning of the trifluoromethyl group. Replacement of the aromatic residue would have the benefit of significantly reducing the lipophilicity and molecular weight. In addition, we speculated that this change might be significantly less tolerated for Plk1 and thus lead to an improved selectivity window.

Synthesis and profiling of truncated inhibitors

To explore this design rationale we prepared a compound in which the benzyl ether moiety was replaced by an allylic ether bearing the desired *Z* configuration. Pleasingly, aminopyridine ***rac*-21** was roughly equipotent compared to the parent compound: the Nek2 IC₅₀ value was found to be 0.073 μM, the LE value was 0.29 with a CLogP reduced to 4.37 (Table 4). These figures compared well with those associated with benzyl ether ***rac*-17j** and demonstrate that replacing the aromatic ring with a smaller allyl ether is tolerated and afforded a compound with better LE and lower CLogP (aminopyridine ***rac*-21**, Table 4). The crystal structure of ***rac*-21** bound to Nek2 confirmed that the binding mode was as expected (Figure 2E and 2F). The reduced bulk of the allylic ether compared to the benzyl ether allowed the binding of an ordered water molecule within the active site, although this apparently had little impact on the potency of inhibition. Our previous studies on benzimidazole-based Nek2 inhibitors showed that the *R* configured enantiomer is significantly more potent than the *S* enantiomer.⁶ We therefore separated the two enantiomers of aminopyridine ***rac*-21** through chiral HPLC.¹⁷ The faster eluting enantiomer showed a Nek2 IC₅₀ value of 1.80 μM, more than seventy times weaker than the slower eluting enantiomer, which had an IC₅₀ value of 0.022 μM. Since we have previously shown that the *R* configuration is preferred for Nek2 inhibition, we assigned the *R* configuration to the slower eluting enantiomer, whereas the faster eluting compound was associated to the *S* configuration (Table 4).

Table 4. Alkene series^a

compound		Nek2 IC ₅₀ (μM)	LE	Plk1	IC ₅₀	CLog
----------	--	----------------------------	----	------	------------------	------

				(μM)	P
<i>rac</i> -17j		0.059 ± 0.016	0.26	1.32 ± 0.34	5.42
<i>rac</i> -21		0.073 ± 0.011	0.29	8.41	4.37
(<i>S</i>)-21		1.80 ± 0.14	0.23	>50	4.37
(<i>R</i>)-21		0.022 ± 0.004	0.31	5.82 (3.92, 7.72)	4.37

^a Results are mean (\pm SD) for $n \geq 3$, or mean values of two independent determinations with individual determinations in parentheses or samples run $n = 1$; compounds are racemic unless otherwise stated.

It is worth noting that the high activity against Nek2 is accompanied by substantial improvement of lipophilicity and LE (compare compounds *rac*-17j, *rac*-21 and (*R*)-21, Table 4). To our knowledge, compound (*R*)-21 is the most potent reversible Nek2 inhibitor reported to date.

Kinase selectivity

Table 5. Selectivity profile^a

compound		Nek2 IC ₅₀ (μM)	Plk1 IC ₅₀ (μM)	MPS1 IC ₅₀ (μM)	AurA IC ₅₀ (μM)	CDK2 IC ₅₀ (μM)	CLogP
17a		0.12 ± 0.01	1.56 ± 0.18	3.06 ± 0.40	7.93 (8.44, 7.41)	2.74 (2.88, 2.60)	5.47
(<i>R</i>)-17j		0.037	0.82 (0.82, 0.83)	4.81 ± 0.31	8.81 ± 0.58	26.6 (26.7, 26.4)	5.42
(<i>S</i>)-21		1.80 ± 0.14	>50	7.12 ± 0.13	2.33 ± 0.23	0.53 (0.52, 0.53)	4.37
(<i>R</i>)-21		0.022 ± 0.004	5.82 (3.92, 7.72)	8.47 ± 0.23	4.94 ± 0.73	4.57 (4.77, 4.36)	4.37

^a Results are mean (± SD) for $n \geq 3$, or mean values of two independent determinations with individual determinations in parentheses or samples run $n = 1$; compounds are racemic unless otherwise stated.

An assessment of the selectivity profile for key compounds was then carried out on four kinases involved in the mitotic machinery: Plk1, MPS1, AurA and CDK2 (Table 5). For comparison purposes, aminopyridine **17j** was prepared as a single enantiomer in the *R* configuration (compound (*R*)-**17j**, Table 5). In general, all the compounds showed a good level of selectivity. However, as anticipated, the

truncated compound **(R)-21** showed significantly improved selectivity against Plk1 (compare aminopyridines **17a** and **(R)-17j** and **(R)-21**, Table 5). Selectivity data on MPS1 inhibition showed a similar trend, with the alkene compounds showing higher IC₅₀ values (Table 5). Finally, all the compounds demonstrated low activity towards Aurora A and CDK2 with the exception of the weak Nek2 inhibitor **(S)-21**, which inhibited CDK2 with an IC₅₀ value of 0.53 μ M (Table 5). Further profiling of compound **(R)-21** was performed against a panel of 24 kinases using a ProfilerPro 1 kit. Again, at least a 100-fold window of selectivity was observed in most cases even though a few cell cycle-unrelated kinases showed a more pronounced inhibition (Table 6). Despite this, we concluded that aminopyridine **(R)-21** fulfils our requirements in terms of both potency and selectivity (IC₅₀ value of 0.022 μ M, Gini coefficient¹⁸ = 0.514 (1 μ M), Table 5 and 6).

Table 6. Selectivity data for **(R)-21** against a panel of kinases.^a

kinase	% of inhibition @ 1 μ M	IC ₅₀ (μ M)
MAPKAPK2	6	
AurA	19	
PKCz	12	
RSK1	29	
PRAK	7	
Erk1	2	
PKD2	77	0.33
CH1d	67	0.43
CHK1	11	
ABL	46	1.11
FYN	57	0.75
LYN	43	1.36
CHK2	32	2.00
MET	46	1.17

LCK	89	0.11
SRC	51	0.84
GSK3b	93	0.07
Erk2	11	
PKA	12	
AKT2	0	
INSR	0	
p38a	0	
AKT1	3	
MSK1	25	

^a 1 μ M (**R**)-**21**, 30 min. pre-incubation compound + enzyme, assay run at apparent ATP K_m for each enzyme.

Cellular profiling of *rac*-**3**, (**R**)-**17j**, (**R**)-**21** and (**S**)-**21**

Next, we evaluated the ability of aminopyridines (**R**)-**17j**, (**R**)-**21** and (**S**)-**21** to inhibit Nek2 in cells by analyzing the effect of these compounds on phosphorylation of C-Nap1. As described in the introduction, the centrosomal protein C-Nap1 has been shown to be a substrate of Nek2 and S-2179 was identified by mass spectrometry as a site that was phosphorylated by Nek2 *in vitro*. We therefore raised rabbit polyclonal antibodies against this phosphorylation site that could act as a direct marker of Nek2 activity in cells. The specificity of this pC-Nap1 antibody was confirmed using S2179A mutants and by RNAi depletion of either C-Nap1 or Nek2 in cells.¹⁹ Briefly, osteosarcoma U2OS cells were synchronized using aphidicolin for 16-18 h, as Nek2 activity is elevated in S and G2 phase, and shortly after release treated with compounds at different concentrations. Phosphorylation of C-Nap1 was determined by measuring the intensity of centrosome staining following immunofluorescence microscopy with the pC-Nap1 antibody. Centrosomes, detected with γ -tubulin antibodies, were scored as positive for pC-Nap1 staining on an IN Cell Analyzer 1000 if the fluorescence intensity was above a defined threshold. The IN Cell Investigator Developer Toolbox (GE Healthcare) was used to analyze the data. All compounds were tested at least twice.²⁰

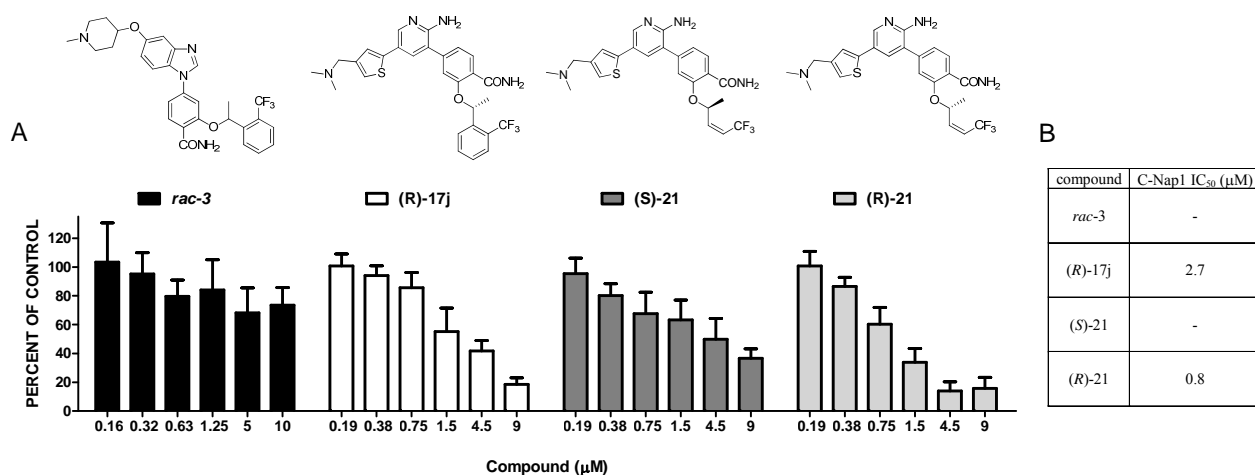


Figure 3. C-Nap1 phosphorylation inhibition activity for *rac*-3, (*R*)-17j, (*S*)-21 and (*R*)-21. (A) C-Nap1 phosphorylation experiments (results are expressed as the percent of cells with pC-Nap1 spot(s) as a percent of DMSO (1%) control). Error bars represent the standard deviation of six replicates obtained in two separate experiments. (B) IC₅₀ values for C-Nap1 phosphorylation inhibition calculated for compounds achieving more than 40 % inhibition.

Representative results are shown in Figure 3A. Pleasingly, aminopyridine (*R*)-21 indeed showed concentration-dependent down-regulation of C-Nap1 phosphorylation with an IC₅₀ value of 0.8 μM (Figure 3B). The approximately 40-fold drop of the IC₅₀ values compared to the biochemical assays can be attributed to the higher ATP concentrations in cells and is not uncommon for ATP competitive kinase inhibitors. The corresponding benzyl ether compound (*R*)-17j also showed an effect in this assay albeit at a slightly higher concentration leading to an IC₅₀ of 2.7 μM (Figure 3A and 3B). The somewhat reduced activity might be due to the more lipophilic character of (*R*)-17j, causing binding to other components and so reducing the effective concentration. It is worth noting that benzimidazole *rac*-3 did not show any significant modulation of C-Nap1 phosphorylation in this assay even at high concentrations (Figure 3A). Finally we tested aminopyridine (*S*)-21, a much weaker biochemical inhibitor of Nek2, in this assay. Indeed, this compound showed significantly less suppression of C-Nap1 phosphorylation and a flatter concentration dependency (Figure 3). We attributed the weak effect of (*S*)-21 in this assay to residual Nek2 activity, however other factors, such as inhibition of upstream kinases,

might also play a role. The flat concentration dependency could also be explained by the hypothesis that the weak effect of aminopyridine (**S**)-**21** in this assay is due to modulation of different targets, very likely with different IC₅₀ values. Overall, these experiments showed that (**R**)-**17j**, and particularly (**R**)-**21**, inhibit the phosphorylation of C-Nap1, a cellular substrate of Nek2, in a concentration dependent manner. Next, we tested the effect of benzimidazole *rac*-**3** and of aminopyridines (**R**)-**17j**, (**S**)-**21**, and (**R**)-**21** on the growth of a panel of cancer cell lines. We determined the concentration required to inhibit the growth by 50% (GI₅₀) after 96 h. However, we did not observe any clear trends between biochemical and C-Nap1 assay on one hand and antiproliferative effect on the other hand (Table 7). These results suggest, at least in the case of the weak Nek2 inhibitor (**S**)-**21**, that inhibition of other targets is responsible for the toxicity against the cancer cell lines after long term exposure. Similar off-target inhibition might also contribute to the antiproliferative effects of aminopyridines (**R**)-**17j** and (**R**)-**21**, albeit to a lesser degree.

The data collected in the C-Nap1 phosphorylation assay combined with the profiling against other prominent cell cycle kinases suggest that aminopyridine (**R**)-**21** can serve as a valuable tool for investigating the role of Nek2 in the cell cycle and its function in mitotic organization. It will be particularly useful in short term experiments using synchronized cell populations aiming to identify additional substrates and functions of Nek2.

Lastly, racemic aminopyridines *rac*-**17j** and *rac*-**21** showed medium to high permeability at physiological pH in a parallel artificial membrane assay (PAMPA, 15.2×10^{-6} and 27.6×10^{-6} cm/s respectively) as well as high metabolic degradation.²¹

Table 8. GI₅₀ values for compounds *rac*-**3**, (**R**)-**17j**, (**S**)-**21** and (**R**)-**21**^a

compound	U2OS GI ₅₀ (μM)	MDA-MB-231 GI ₅₀ (μM)	HeLa GI ₅₀ (μM)	MCF7 GI ₅₀ (μM)
<i>rac</i> - 3	2.96 (3.73, 2.17)	4.95 (4.81, 5.08)	1.20 ± 0.23	2.03 (1.68, 2.38)

(<i>R</i>)-17j	0.48 (0.51, 0.45)	0.95 (0.87, 1.02)	0.14 ± 0.06	0.22 (0.21, 0.23)
(<i>S</i>)-21	2.17 (2.17, 2.16)	7.25 (6.40, 8.09)	0.44 ± 0.13	5.42 (4.72, 6.12)
(<i>R</i>)-21	1.82 (2.22, 1.41)	4.16 (3.94, 4.38)	0.59 ± 0.06	2.17 (2.03, 2.31)

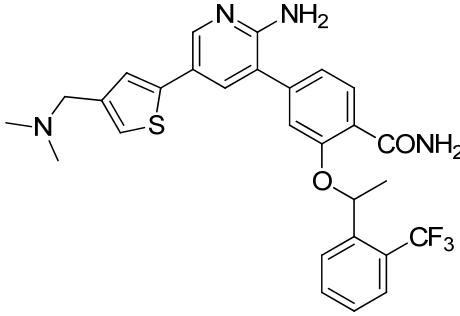
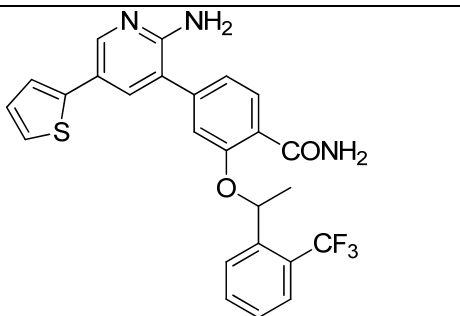
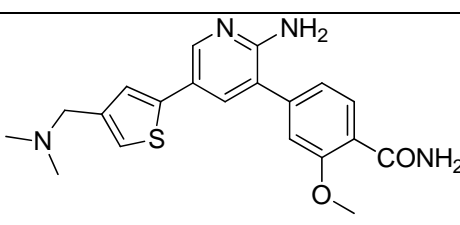
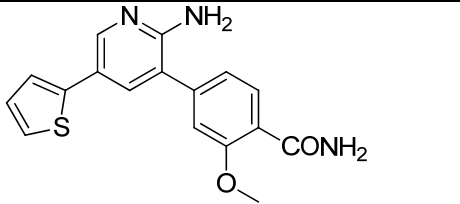
^a Results are mean (± SD) for $n \geq 3$, or mean values of two independent determinations with individual determinations in parentheses or samples run $n = 1$; compounds are racemic unless otherwise stated.

Confirmation of non linear SAR

Finally, we were interested in investigating whether the non-additive SAR observed in the benzimidazole series is also translated in the aminopyridine series. As described above, we previously found that in order to attain high level of Nek2 inhibition, the two key pharmacophoric elements (namely the amino group and the substituted benzylic ether, see Figure 1) had to be present at the same time.⁶ Thus, three truncated analogues of aminopyridine **rac-17j** were prepared, lacking the amino group, the benzylic ether or lacking both groups at the same time. The results show that loss of either of these moieties lead to a sharp decrease in activity to a level observed for the core compound **17i** (Table 8). This confirms that neither of the two substituents significantly improves Nek2 activity on its own (compare core compound **17i** with aminopyridines **17h** or **17k**, IC₅₀ values of 10.5, 9.0 and 2.26 μM, respectively, Table 8).

Table 8. Non-additive SAR^a

compound		Nek2 (μM)	IC ₅₀	LE	CLogP
----------	--	--------------	------------------	----	-------

<i>rac</i> -17j		0.059 0.016	±	0.26	5.42
17h		9.0 ± 1.6		0.20	5.35
17k		2.26 ± 0.36		0.29	2.52
17i		10.5 ± 0.28		0.30	2.45

^a Results are mean (± SD) for $n \geq 3$, or mean values of two independent determinations with individual determinations in parentheses or samples run $n = 1$; compounds are racemic unless otherwise stated.

Instead, a large jump in activity (ca. 200-fold) takes place when both substituents are present in *rac*-**17j**, as previously observed in the benzimidazole series. These results confirm that the non-linear SAR observed for benzimidazoles translates into the aminopyridine series.

Conclusions

Starting from two different sets of Nek2 ligands, we designed a series of hybrid inhibitors. Using structure-based design we optimized Nek2 potency, kinase selectivity, lipophilicity and ligand efficiency to the desired range, ultimately culminating in aminopyridine (*R*)-**21**. To our knowledge (*R*)-**21** is the most potent reversible inhibitor of Nek2 known to date. In our cellular assay, compound (*R*)-**21**

showed a concentration dependent inhibition of phosphorylation of C-Nap1, a known substrate of Nek2. Gratifyingly, aminopyridine (**R**)-**21** also showed sufficient selectivity against the most relevant cell cycle kinases and will therefore make for a useful tool compound to probe the role of Nek2 in cell cycle control. The results of these experiments will be reported in due course.

Experimental section

General Chemistry Information. Starting materials, reagents and solvents for reactions were reagent grade and used as purchased. Chromatography solvents were HPLC grade and were used without further purification. Thin layer chromatography (TLC) analysis was performed using Merck silica gel 60 F-254 thin layer plates. Flash column chromatography was carried out using columns pre-packed with 40-63 μm silica. NMR spectra were recorded on a Bruker Avance 500 MHz spectrometer and samples were referenced to the appropriate internal nondeuterated solvent peak. The data is given as follows: chemical shift (δ) in ppm, multiplicity (where applicable), coupling constants (J) in Hz (where applicable) and integration (where applicable). LCMS analyses were performed on a Micromass LCT/Waters Alliance 2795 separations module HPLC system with a Merck Chromolith SpeedROD RP-18e 50 x 4.6mm column at a temperature of 22 °C. The following solvent system, at a flow rate of 2 mL/min, was used: solvent A: methanol; solvent B: 0.1% formic acid in water. Gradient elution was as follows: 1:9 (A:B) to 9:1 (A:B) over 2.25 min., 9:1 (A:B) for 0.75 min. then reversion back to 1:9 (A:B) over 0.3 min., 1:9 (A:B) for 0.2 min. Detection was carried out with a Waters 2487 Dual λ Absorbance Detector (detecting at 254nm) and ionisation was electrospray (ESI). Some LCMS and all HRMS analyses were performed on a Agilent 1200 series HPLC system with a Merck Chromolith SpeedROD RP-18e 50x4.6mm column at a temperature of 22 °C. The following solvent system, at a flow rate of 2 mL/min, was used: solvent A: methanol; solvent B: 0.1% formic acid in water. Gradient elution was as follows: 1:9 (A:B) to 9:1 (A:B) over 2.5 min., 9:1 (A:B) for 1 min. then reversion back to 1:9 (A:B) over 0.3 min., 1:9 (A:B) for 0.2 min. This was connected to a Agilent 6200 Time of Flight (ToF) mass spectrometer (simultaneous ESI and APCI or ESI only) with detection at 254nm. The following reference masses were used for HRMS analysis: Caffeine $[\text{M} + \text{H}]^+ = 195.087652$, reserpine $[\text{M} + \text{H}]^+$

= 609.280657 and (1H,1H,3H-tetrafluoropentoxo)phosphazene $[M + H]^+ = 922.009798$. The purity of final compounds was determined by HPLC as described above and is $\geq 95\%$ unless specified otherwise.

Methyl 4-bromo-2-hydroxybenzoate 6 A solution of 4-bromo-2-hydroxybenzoic acid **5** (5.00 g, 23.04 mmol) in MeOH (20 mL) was treated with sulfuric acid (1.7 mL). The mixture was refluxed for 24 h, poured onto ice-water and extracted with DCM. The combined organics were washed with satd aqueous NaHCO_3 , dried (Na_2SO_4) and concentrated to give ester **6** (3.97 g, 75%). ^1H NMR (500 MHz, CDCl_3) δ 10.82 (s, 1H), 7.70 (d, $J = 8.5$ Hz, 1H), 7.20 (d, $J = 1.9$ Hz, 1H), 7.04 (dd, $J = 8.5, 1.9$ Hz, 1H), 3.97 (s, 3H).

Methyl 4-bromo-2-((4-methoxybenzyl)oxy)benzoate 12a A solution of phenol **6** (1.70 g, 7.36 mmol), 4-methoxybenzyl alcohol (1.29 g, 9.30 mmol) and triphenylphosphine (2.81 g, 10.71 mmol) in DCM (35 mL) was cooled at 0 °C and treated with di-*tert*-butyl azodicarboxylate (2.45 g, 10.65 mmol). The reaction was allowed to reach rt and stirred overnight. The mixture was diluted with DCM and quenched with water. The organic layer was separated and extracted with DCM. The combined organics were dried (Na_2SO_4), concentrated and purified by Biotage column chromatography (0–7% EtOAc/cyclohexane) to give ether **12a** (2.04 g, 79%). LCMS (ESI) m/z 373 ($M+\text{Na}$). ^1H NMR (500 MHz, CDCl_3) δ 7.70 (d, $J = 8.3$ Hz, 1H), 7.43 – 7.40 (m, 2H), 7.20 (d, $J = 1.8$ Hz, 1H), 7.15 (dd, $J = 8.3, 1.8$ Hz, 1H), 6.96 – 6.93 (m, 2H), 5.11 (s, 2H), 3.89 (s, 3H), 3.83 (s, 3H).

Methyl 4-(2-amino-5-bromopyridin-3-yl)-2-((4-methoxybenzyl)oxy)benzoate 14b A solution of bromide **12a** (1.10 g, 3.13 mmol), bis(pinacolato)diboron (1.20 g, 4.72 mmol), potassium acetate (925 mg, 9.44 mmol) and 1,1'-bis(diphenylphosphino)ferrocene]dichloropalladium(II)·DCM (130 mg, 0.16 mmol) in DMF (15 mL) was stirred at 100 °C under microwave irradiation for 1 h 30 min. The reaction was quenched with brine and extracted with AcOEt. The combined organics were washed with brine, dried (Na_2SO_4), and concentrated to afford the crude boronic ester **13a**.

A solution of crude boronic ester **13a** (ca. 3.13 mmol), sodium bicarbonate (480 mg, 5.71 mmol), 1,1'-bis(diphenylphosphino)ferrocene]dichloropalladium(II)·DCM (125 mg, 0.15 mmol) and 5-bromo-3-

iodopyridin-2-amine (850 mg, 2.84 mmol) in DMF/water (8/1, 15 mL) was stirred at 100 °C under microwave irradiation for 1 h 30 min. The reaction was quenched with brine and extracted with EtOAc. The combined organics were washed with brine, dried (Na₂SO₄), concentrated and purified by Biotage column chromatography (0–30% EtOAc/cyclohexane) to give bromopyridine **14b** (1.02 g, 81%). HRMS (ESI) *m/z* calcd for C₂₁H₂₀BrN₂O₄ (M+H) 443.0601, found 443.0617. ¹H NMR (500 MHz, CDCl₃) δ 8.13 (d, *J* = 2.4 Hz, 1H), 7.90 (d, *J* = 7.8 Hz, 1H), 7.45 (d, *J* = 2.4 Hz, 1H), 7.43 – 7.40 (m, 2H), 7.07 – 7.04 (m, 2H), 6.95 – 6.92 (m, 2H), 5.17 (s, 2H), 4.57 (br. s, 2H), 3.94 (s, 3H), 3.83 (s, 3H).

Methyl 4-(2-amino-5-(4-((dimethylamino)methyl)thiophen-2-yl)pyridin-3-yl)-2-((4-methoxybenzyl)oxy)benzoate 16l A solution of bromide **14b** (1.01 g, 2.28 mmol), bis(pinacolato)diboron (870 mg, 3.43 mmol), potassium acetate (680 mg, 6.94 mmol) and 1,1'-bis(diphenylphosphino)ferrocene]dichloropalladium(II)·DCM (200 mg, 0.25 mmol) in DMF (11 mL) was stirred at 100 °C under microwave irradiation for 1 h 30 min. The reaction was quenched with brine and extracted with AcOEt. The combined organics were washed with brine, dried (Na₂SO₄), and concentrated to afford the crude boronic acid **15b**.

A solution of crude boronic acid **15b** (ca. 2.28 mmol), 1-(5-bromothiophen-3-yl)-*N,N*-dimethylmethanamine¹³ (1.0 g, 4.54 mmol), tetrakis(triphenylphosphine)palladium(0) (250 mg, 0.22 mmol) and sodium carbonate (485 mg, 4.58 mmol) in DME/water (8/1, 15 mL) was heated to 110 °C under microwave irradiation for 1h. The reaction was quenched with brine and extracted with EtOAc. The combined organics were washed with brine, dried (Na₂SO₄), concentrated and purified by Biotage column chromatography (0–25% MeOH/DCM) to give amine **16l** (569 mg, 50% over two steps). LCMS (ESI) *m/z* 504 (M+H). ¹H NMR (500 MHz, CDCl₃) δ 8.36 (s, 1H), 7.92 (d, *J* = 7.9 Hz, 1H), 7.56 (d, *J* = 2.3 Hz, 1H), 7.44 – 7.41 (m, 2H), 7.24 (s, 1H), 7.14 – 7.10 (m, 3H), 6.97 – 6.91 (m, 2H), 5.19 (s, 2H), 4.59 (br. s, 2H), 3.94 (s, 3H), 3.82 (s, 3H), 3.54 (s, 2H), 2.36 (s, 6H).

Methyl 4-(2-amino-5-(4-((dimethylamino)methyl)thiophen-2-yl)pyridin-3-yl)-2-hydroxybenzoate 18 A solution of phenol ether **16l** (560 mg, 1.11 mmol) in DCM (7 mL) was treated with trifluoroacetic

acid (800 μ L, 10.81 mmol) at 0 °C. After 1 h 30 min. the reaction was brought to pH ca. 5–6 with 1M NaOH and 1M HCl, the aqueous layer separated and extracted with DCM. The combined organic layers were concentrated and purified by Biotage column chromatography (0–15% MeOH/DCM) to give phenol **18** (394 mg, 92%). HRMS (ESI) m/z calcd for C₂₀H₂₂N₃O₃S (M+H) 384.1376, found 384.1391. ¹H NMR (500 MHz, MeOD) δ 8.28 (d, J = 2.4 Hz, 1H), 7.99 (d, J = 8.2 Hz, 1H), 7.68 (d, J = 2.4 Hz, 1H), 7.58 (d, J = 1.4 Hz, 1H), 7.39 (d, J = 1.4 Hz, 1H), 7.10 (d, J = 1.7 Hz, 1H), 7.07 (dd, J = 8.2, 1.7 Hz, 1H), 4.30 (s, 2H), 4.00 (s, 3H), 2.88 (s, 6H).

(\pm)-(Z)-Methyl 4-(2-amino-5-(4-((dimethylamino)methyl)thiophen-2-yl)pyridin-3-yl)-2-((5,5,5-trifluoropent-3-en-2-yl)oxy)benzoate **20** A solution of phenol **18** (64 mg, 0.17 mmol), (\pm)-5,5,5-trifluoropent-3-yn-2-ol¹⁴ 20% w/w solution in EtOAc, 0.31 mmol) and triphenylphosphine (70 mg, 0.27 mmol) in DCM (1 mL) was cooled at 0 °C and treated with di-*tert*-butyl azodicarboxylate (60 mg, 0.26 mmol). The reaction was allowed to reach rt and stirred overnight. Additional batches of reagents were added as required until the reaction reached completion. The mixture was diluted with DCM and quenched with water. The organic layer was separated and extracted with DCM. The combined organics were dried (Na₂SO₄), concentrated and purified by Biotage column chromatography (0–15% MeOH/DCM) to give ether **19**.

A solution of ether **19** (ca. 0.050 mmol) in MeOH (2 ml) was treated with palladium on calcium carbonate (poisoned with lead (Lindlar's catalyst), 5% w/w, 5 mg, 2.4 μ mol) and stirred in an atmosphere of hydrogen overnight. Additional batches of palladium on calcium carbonate (poisoned with lead, 5% w/w, 7 mg, 3.3 μ mol) were added and the mixture stirred in an atmosphere of hydrogen until completion. The mixture was filtrated over Celite washing with MeOH, the solvent removed under reduced pressure and the residue purified by semi-preparative reverse phase HPLC (Phenomenex Gemini C18 column; 15 min. gradient 25-50% MeOH/water, 0.1% formic acid; 5 mL/min.) to give alkene **20** (12 mg, 14% over two steps). HRMS (ESI) m/z calcd for C₂₅H₂₇F₃N₃O₃S (M+H) 506.1720, found 506.1701. ¹H NMR (500 MHz, MeOD) δ 8.29 (d, J = 2.4 Hz, 1H), 7.88 (d, J = 8.0 Hz, 1H), 7.65

(d, $J = 2.4$ Hz, 1H), 7.56 (s, 1H), 7.37 (d, $J = 1.5$ Hz, 1H), 7.22 (dd, $J = 8.0, 1.5$ Hz, 1H), 7.17 (s, 1H), 6.27 (dd, $J = 12.1, 8.7$ Hz, 1H), 5.94 – 5.85 (m, 1H), 5.49 – 5.45 (m, 1H), 4.24 (s, 2H), 3.92 (s, 3H), 2.83 (s, 6H), 1.55 (d, $J = 6.4$ Hz, 3H).

(±)-(Z)-4-(2-Amino-5-(4-((dimethylamino)methyl)thiophen-2-yl)pyridin-3-yl)-2-((5,5,5-trifluoropent-3-en-2-yl)oxy)benzamide **rac-21** Ester **20** (16 mg, 0.032 mmol) was treated with ammonia in methanol (7M, 4 mL) and heated to 75 °C in a closed-cap vial for 4 days. The mixture was concentrated, and the residue purified by Biotage column chromatography (0–15% MeOH/DCM) to give amide **rac-21** (9 mg, 56%). HRMS (ESI) m/z calcd for $C_{24}H_{26}F_3N_4O_2S$ (M+H) 491.1723, found 491.1749. 1H NMR (500 MHz, $(CD_3)_2SO$) δ 8.27 (d, $J = 2.4$ Hz, 1H), 7.88 (d, $J = 8.0$ Hz, 1H), 7.65 (br. s, 1H), 7.57 (br. s, 1H), 7.53 (d, $J = 2.4$ Hz, 1H), 7.26 (d, $J = 1.5$ Hz, 1H), 7.22 (dd, $J = 8.0, 1.5$ Hz, 1H), 7.18 (s, 1H), 7.09 (d, $J = 1.5$ Hz, 1H), 6.41 (dd, $J = 12.1, 8.5$ Hz, 1H), 6.09 – 6.04 (m, 1H), 5.98 (s, 2H), 5.58 – 5.54 (m, 1H), 3.36 (s, 2H), 2.15 (s, 6H), 1.53 (d, $J = 6.3$ Hz, 3H).

Aminopyridine **rac-21** was separated into enantiomers by chiral HPLC (LUX cellulose II; 90% acetonitrile/2-propanol; 1 mL/min):

Peak 1: retention time 12.3 min: (S)-(Z)-4-(2-Amino-5-(4-((dimethylamino)methyl)thiophen-2-yl)pyridin-3-yl)-2-((5,5,5-trifluoropent-3-en-2-yl)oxy)benzamide (S)-**21** HRMS (ESI) m/z calcd for $C_{24}H_{26}F_3N_4O_2S$ (M+H) 491.1723, found 491.1722. 1H NMR (500 MHz, $(CD_3)_2SO$) δ 8.27 (d, $J = 2.4$ Hz, 1H), 7.88 (d, $J = 8.0$ Hz, 1H), 7.65 (br. s, 1H), 7.57 (br. s, 1H), 7.53 (d, $J = 2.4$ Hz, 1H), 7.26 (d, $J = 1.5$ Hz, 1H), 7.22 (dd, $J = 8.0, 1.5$ Hz, 1H), 7.18 (s, 1H), 7.09 (d, $J = 1.5$ Hz, 1H), 6.41 (dd, $J = 12.1, 8.5$ Hz, 1H), 6.09 – 6.04 (m, 1H), 5.98 (s, 2H), 5.58 – 5.54 (m, 1H), 3.36 (s, 2H), 2.15 (s, 6H), 1.53 (d, $J = 6.3$ Hz, 3H).

Peak 2: retention time 15.2 min: (R)-(Z)-4-(2-Amino-5-(4-((dimethylamino)methyl)thiophen-2-yl)pyridin-3-yl)-2-((5,5,5-trifluoropent-3-en-2-yl)oxy)benzamide (R)-**21** HRMS (ESI) m/z calcd for $C_{24}H_{26}F_3N_4O_2S$ (M+H) 491.1723, found 491.1719. 1H NMR (500 MHz, $(CD_3)_2SO$) δ 8.27 (d, $J = 2.4$ Hz, 1H), 7.88 (d, $J = 8.0$ Hz, 1H), 7.65 (br. s, 1H), 7.57 (br. s, 1H), 7.53 (d, $J = 2.4$ Hz, 1H), 7.26 (d, $J =$

1.5 Hz, 1H), 7.22 (dd, $J = 8.0, 1.5$ Hz, 1H), 7.18 (s, 1H), 7.09 (d, $J = 1.5$ Hz, 1H), 6.41 (dd, $J = 12.1, 8.5$ Hz, 1H), 6.09 – 6.04 (m, 1H), 5.98 (s, 2H), 5.58 – 5.54 (m, 1H), 3.36 (s, 2H), 2.15 (s, 6H), 1.53 (d, $J = 6.3$ Hz, 3H).

Biochemical assays. Nek2 and Plk1 biochemical assays were performed as reported previously. MPS1, AurA and CDK2 counterscreen assays were carried out using similar procedures.^{5,6}

Cellular assays. CellTiter-Blue Assay for Growth Inhibition

U2OS human osteosarcoma cells (American Type Culture Collection, Manassas, Virginia, United States) were grown in McCoy's 5A medium supplemented with 1.5 mM L-glutamine, 25 mM HEPES, 2% penicillin/streptomycin (Invitrogen, Paisley, United Kingdom), and 10% fetal bovine serum (Biosera, Ringmer, East Sussex, United Kingdom). Cells were maintained in a humidified atmosphere of 5% CO₂ at 37°C. The medium was aspirated and the cells were washed with PBS (Invitrogen, Paisley, United Kingdom), trypsinized (Internal supply, 0.25% versene trypsin with EDTA), neutralized, and counted. Cells were seeded into 384-well clear tissue culture treated microtiter plates (Corning B.V. Life Sciences, Amsterdam, The Netherlands) at 200 cells per well in a 45 µL volume of the respective media. Columns 1 and 24 had no cells added and were plated with 45 µL of media alone. Cells were incubated at 37°C / 5% CO₂. At 24 hours after plating, test compounds, Etoposide as positive control (Sigma-Aldrich, Gillingham, Dorset, United Kingdom), or DMSO at 1% v/v final concentration (Fisher Scientific, Loughborough, Leicestershire, United Kingdom) were dispensed using an Echo liquid handling system (Labcyte, Dublin, Ireland). After 92 hours, 5 µL of CellTiter-Blue Reagent (Promega, Southampton, United Kingdom) was added to the cells using a Multidrop dispenser (Thermo Electron, Basingstoke, Hants, United Kingdom) and incubated for 4 hours in a humidified atmosphere of 5% CO₂ at 37°C. After the incubation, the plates were placed at room temperature for 40 minutes before fluorescence was recorded (560_{Ex}/590_{Em}) on an EnVision 2103 plate reader (PerkinElmer Life Sciences). Data were plotted as percentage of DMSO control against compound concentration using GraphPad Prism 5 Software. The 50% growth inhibition (GI₅₀) was calculated as

the compound concentration required to reduce the cell number by 50% compared with the DMSO control.

MDA-MB-231 cells (American Type Culture Collection, Manassas, Virginia, United States) were grown in RPMI medium (Invitrogen, Paisley, United Kingdom) supplemented with 2% penicillin/streptomycin and 10% fetal bovine serum.

HeLa cells (American Type Culture Collection, Manassas, Virginia, United States) were grown in Dulbecco's Modified Eagle Medium (Invitrogen, Paisley, United Kingdom) supplemented with 2% penicillin/streptomycin and 10% fetal bovine serum.

MCF7 cells (American Type Culture Collection, Manassas, Virginia, United States) were grown in Dulbecco's Modified Eagle Medium supplemented with 2% penicillin/streptomycin and 10% fetal bovine serum. They were plated at 800 cells per well.

Phosphorylated C-Nap1 in Cell Assay

U2OS human osteosarcoma cells (American Type Culture Collection, Manassas, Virginia, United States) were grown in McCoy's 5A medium supplemented with 1.5 mM L-glutamine, 25 mM HEPES, 2% penicillin/streptomycin (Invitrogen, Paisley, United Kingdom), and 10% fetal bovine serum (Biosera, Ringmer, East Sussex, United Kingdom). Cells were maintained in a humidified atmosphere of 5% CO₂ at 37°C. The medium was aspirated and the cells were washed with PBS (Invitrogen, Paisley, United Kingdom), trypsinized (Internal supply, 0.25% versene trypsin with EDTA), neutralized, and counted. Cells were seeded into 96-well black clear bottom tissue culture treated microtiter plates (PerkinElmer Life Sciences, Waltham, Massachusetts, USA) at 10,000 cells per well in a 180 µL volume of media. Cells were incubated for 24 hours at 37°C / 5% CO₂ after which Aphidicolin (Sigma-Aldrich, Gillingham, Dorset, United Kingdom) was added to all wells for cell synchronization at a final concentration of 2 µg/mL for 16-18 hours. The cells were then released into 180 µL of fresh media. Simultaneously, the cells were treated in triplicate wells with test compound in DMSO at 1% v/v final concentration (Fisher Scientific, Loughborough, Leicestershire, United Kingdom) and incubated for 3 hours. 1% DMSO final concentration was used as a negative control.

The cells were then fixed for 15 minutes at 2-8°C with 50 µL cold 100% methanol. The plates were washed once with 100 µL PBS before blocking non-specific binding with 50 µL 5% w/v Bovine Serum Albumin (Sigma-Aldrich, Gillingham, Dorset, United Kingdom) in PBS for 1 hour at room temperature with gentle agitation. A rabbit polyclonal antibody raised to phosphorylated C-Nap1 (generated by Peptide Specialty Laboratories, GmbH, Heidelberg) was added at a dilution of 1:750, and a monoclonal antibody raised to the centrosomal marker γ -tubulin (Sigma-Aldrich, Gillingham, Dorset, United Kingdom) was added at a dilution of 1:500 for 1 hour at room temperature with gentle agitation. Following a further wash with PBS, Alexa fluor 488 goat anti-rabbit IgG and Alexa fluor 568 goat anti-mouse IgG (Invitrogen, Paisley, United Kingdom) were added at a final concentration of 4 µg/mL in 5% BSA/PBS for 1 hour at room temperature under gentle agitation. After another wash with PBS, the nuclear stain DAPI (Invitrogen, Paisley, United Kingdom) was added at a final concentration of 2.5 µg/mL in PBS for 10 minutes at room temperature with gentle agitation. The plate was washed in PBS once again and refrigerated until ready to image. The assay plates were read on the IN Cell Analyzer 1000 using the Workstation 1000 acquisition software (GE Healthcare, Amersham, United Kingdom). The instrument was equipped with a 20X dry Nikon objective, a D360/40X DAPI excitation filter, an HQ480/40X FITC excitation filter, an HQ565/30X excitation filter, an HQ460/40M bandwidth emission filter, an HQ535nm/50M bandwidth emission filter, and an HQ620nm/60M bandwidth emission filter. The exposure times were consistently 200 ms in the DAPI channel, 400 ms in the FITC channel, and 1000 ms in the red channel. Fifteen fields of view were imaged in all wells. IN Cell Investigator Developer Toolbox (GE Healthcare) was used to analyze the assay data. The algorithm was written to identify the DAPI-stained nuclei, and then segment the cells setting a small collar around the nuclei as the centrosomal inclusion area. The γ -tubulin-identified centrosomes and phosphorylated C-Nap1 spots were chosen based on size and pixel intensity and were only counted if they were located within the centrosomal inclusion area. A “One to One link” was written into the protocol so that only phosphorylated C-Nap1 spots colocalized with the centrosomal γ -tubulin were counted. Data were

plotted as percentage of DMSO control against compound concentration using GraphPad Prism 5 Software.

Acknowledgement. We acknowledge NHS funding to the NIHR Biomedical Research Centre and funding from Cancer Research UK programme grant number C309/A8274. AMF acknowledges support from Cancer Research UK, The Wellcome Trust and the Association for International Cancer Research. RB acknowledges support from Cancer Research UK (grant C24461/A10285 and infrastructure support for Structural Biology at the ICR), a Royal Society Research Fellowship and the Career Development Programme of the ICR. We are thankful to Prof. Julian Blagg, Prof. Roger Griffin, Prof. Herbie Newell, Dr. Ian Collins and Prof. Paul Workman for helpful discussions. We also thank Dr. Amin Mirza, Mr. Meirion Richards and Dr. Maggie Liu for their help with HPLC, NMR and mass spectrometry. Ms Jessica Schmitt is acknowledged for biochemical assays. We are indebted to the staff of ESRF beamline ID29 as well as our many colleagues of the Section of Structural Biology (ICR in London) for their support during data collection.

Supporting Information Available: Experimental procedures, analytical data for final compounds **11**, **17** and intermediates, a summary of crystallographic analysis of aminopyridine *rac*-**17j** and *rac*-**21**, HPLC traces for compounds **21**, C-Nap1 antibody characterization and pictures of assay plates. This material is available free of charge via the Internet at <http://pubs.acs.org>.

References

¹ O'Regan, L.; Blot, J.; Fry, A. M. Mitotic regulation by NIMA-related kinases. *Cell Div.* **2007**, 2, 25–36.

² a) Lou, Y.; Yao, J.; Zereszki, A.; Dou, Z.; Ahmed, K.; Wang, H.; Hu, J.; Wang, Y.; Yao, X. NEK2A interacts with MAD1 and possibly functions as a novel integrator of the spindle checkpoint signaling. *J. Biol. Chem.* **2004**, 279, 20049–20057; b) Chen, Y.; Riley, D. J.; Zheng, L.; Chen, P. L.; Lee, W. H.

Phosphorylation of the mitotic regulator protein Hec1 by Nek2 kinase is essential for faithful chromosome segregation. *J. Biol. Chem.* **2002**, 277, 49408–49416.

³ a) Henise, J. C.; Taunton, J. Irreversible Nek2 kinase inhibitors with cellular activity. *J. Med. Chem.* **2011**, 54, 4133–4146; b) Mardin, B. R.; Lange, C. L.; Baxter, J. E.; Hardy, T.; Scholz, S. R.; Fry, A. M.; Schiebel, E. Components of the Hippo pathway cooperate with Nek2 kinase to regulate centrosome disjunction. *Nat. Cell Biol.* **2010**, 12, 1166–1176.

⁴ a) Fletcher, L.; Cerniglia, G. J.; Nigg, E. A.; Yend, T. J.; Muschel, R. J. Inhibition of centrosome separation after DNA damage: a role for Nek2. *Radiat. Res.* **2004**, 162, 128–135; b) Kokuryo, T.; Senga, T.; Yokoyama, Y.; Nagino, M.; Nimura, Y.; Hamaguchi, M. Nek2 as an effective target for inhibition of tumorigenic growth and peritoneal dissemination of cholangiocarcinoma *Cancer Res.* **2007**, 67, 9637–9642; c) Tsunoda, N.; Kokuryo, T.; Oda, K.; Senga, T.; Yokoyama, Y.; Nagino, M.; Nimura, Y.; Hamaguchi, M. Nek2 as a novel molecular target for the treatment of breast carcinoma. *Cancer Sci.* **2009**, 100, 111–116.

⁵ Whelligan, D. K.; Solanki, S.; Taylor, D.; Thomson, D. W.; Cheung, K. M. J.; Boxall, K.; Mas-Droux, C.; Barillari, C.; Burns, S.; Grummitt, C. G.; Collins, I.; van Montfort, R. L. M.; Aherne, G. W.; Bayliss, R.; Hoelder, S. Aminopyrazine inhibitors binding to an unusual inactive conformation of the mitotic kinase Nek2: SAR and structural characterization. *J. Med. Chem.* **2010**, 53, 7682–7698.

⁶ Solanki, S.; Innocenti, P.; Mas-Droux, C.; Boxall, K.; Barillari, C.; van Montfort, R. L. M.; Aherne, G. W.; Bayliss, R.; Hoelder, S. Benzimidazole inhibitors induce a DFG-out conformation of never in mitosis gene A-related kinase 2 (Nek2) without binding to the back pocket and reveal a nonlinear structure–activity relationship. *J. Med. Chem.* **2011**, 54, 1626–1639.

⁷ Mitsunobu, O. The use of diethyl azodicarboxylate and triphenylphosphine in synthesis and transformation of natural-products. *Synthesis* **1981**, 1–28.

⁸ Ishiyama, T.; Murata, M.; Miyaura, N. Palladium(0)-catalyzed cross-coupling reaction of alkoxydiboron with haloarenes: a direct procedure for arylboronic esters. *J. Org. Chem.* **1995**, *60*, 7508–7510.

⁹ a) Kundo, M.; Khairatkar-Joshi, N.; Nadkarni, S. M.; Pansare, R. M.; Karnik, P. V. Bicyclic heteroaryl derivatives as cannabinoid receptor modulators. (Glenmark pharmaceuticals SA). Patent WO 2007/096764, 2007; b) Binch, H.; Robinson, D.; Miller, A.; Fraysse, D. Pyrrolopyrazines and pyrazolopyrazines useful as inhibitors of protein kinases. (Vertex pharma). Patent WO 2006/058074, 2006.

¹⁰ Miyaura, N.; Suzuki, A. Palladium-catalyzed cross-coupling reactions of organoboron compounds. *Chem. Rev.* **1995**, *95*, 2457–2483.

¹¹ See Supporting Information for detailed procedures.

¹² Hilton, S.; Naud, S.; Caldwell, J. C.; Boxall, K.; Burns, S.; Anderson, V. E.; Antoni, L.; Allen, C. A.; Pearl, L. H.; Oliver, A. W.; Aherne, G. W.; Garrett, M. D.; Collins, I. Identification and characterisation of 2-aminopyridine inhibitors of checkpoint kinase 2. *Bioorg. Med. Chem.* **2010**, *18*, 707–718.

¹³ 1-(5-Bromothiophen-3-yl)-*N,N*-dimethylmethanamine was prepared by reductive amination of the known corresponding aldehyde: Deng, J.; Kerns, J. K.; Jin, Q.; Lin, G.; Lin, X.; Lindenmuth, M.; Neipp, C. E.; Nie, H.; Thomas, S. M.; Widdowson, K. L. Chemical compounds. (Smithkline Beecham Corporation). Patent WO 2007/005534, 2007. See Supporting Information for experimental details.

¹⁴ (±)-5,5,5-trifluoropent-3-yn-2-ol was prepared according to a modified literature method: Yamazaki, T.; Mizutani, K.; Kitazume, T. Modified preparation of trifluoromethylated propargylic alcohols and its application to chiral 2,6-dideoxy-6,6,6-trifluorosugars. *J. Org. Chem.* **1995**, *60*, 6046–6056. See Supporting Information for experimental details.

¹⁵ Whelligan, D. K.; Solanki, S.; Taylor, D.; Thomson, D. W.; Cheung, K. M. J.; Hoelder, S. unpublished results.

¹⁶ a) Rapley, J.; Baxter, J. E.; Blot, J.; Wattam, S. L.; Casenghi, M.; Meraldi, P.; Nigg, E. A.; Fry, A. M. Coordinate regulation of the mother centriole component Nlp by Nek2 and Plk1 protein kinases. *Mol. Cell. Biol.* 2005, 25, 1309–1324; b) for a study on Plk1 inhibitors, see: Emmitte, K. A.; Adjebang, G. M.; Andrews, C. W.; Alberti, J. G.; Bambal, R.; Chamberlain, S. D.; Davis-Ward, R. G.; Dickson, H. D.; Hassler, D. F.; Hornberger, K. R.; Jackson, J. R.; Kuntz, K. W.; Lansing, T. J.; Mook, R. A., Jr.; Nailor, K. E.; Pobanz, M. A.; Smith, S. C.; Sung, C. M.; Cheung, M. Design of potent thiophene inhibitors of polo-like kinase 1 with improved solubility and reduced protein binding. *Bioorg. Med. Chem. Lett.* **2009**, 19, 1694–1697.

¹⁷ See Experimental Section and Supporting Information for details.

¹⁸ Graczyk, P. P. Gini coefficient: a new way to express selectivity of kinase inhibitors against a family of kinases. *J. Med. Chem.* **2007**, 50, 5773–5779.

¹⁹ See Figure S2 in Supporting Information for more details.

²⁰ See Figure S3 in the Supporting Information for samples of the assay readout.

²¹ 87% and 95% respectively of aminopyridines **rac-17j** and **rac-21** were metabolized in MLM after 30 min. Data for the benzimidazole series have been previously published (see ref. 6).

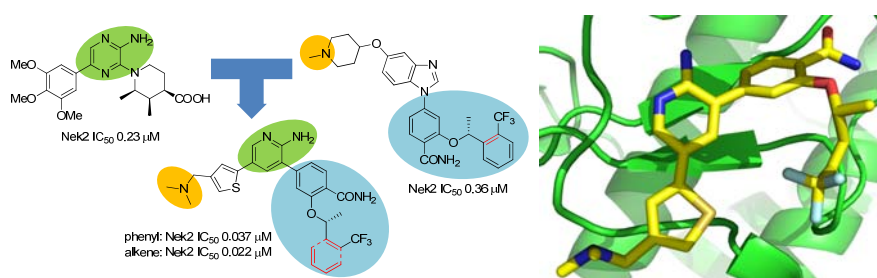


Table of Contents Graphic